

A wide angle view of the Sagittarius dwarf Spheroidal Galaxy. I: VIMOS photometry and radial velocities across Sgr dSph major and minor axis. [★]

G. Giuffrida¹, L. Sbordone^{2,3,4}, S. Zaggia⁵, G. Marconi⁶, P. Bonifacio^{2,3,7}, C. Izzo⁸, T. Szeifert⁶, and R. Buonanno⁹

¹ ASI Science data Center, Via Galileo Galilei, 00044, Frascati, Italy

e-mail: giuffrida@mporzio.astro.it

² CIFIST Marie Curie Excellence Team

³ GEPI, Observatoire de Paris, CNRS, Université Paris Diderot; Place Jules Janssen 92190 Meudon, France

⁴ Max-Planck-Institut für Astrophysik, Karl-Schwarzschild-Str. 1, Postfach 1317, 85741 Garching b. München, Germany

⁵ INAF – Osservatorio Astronomico di Padova Vicolo dell’Osservatorio 5, - 35122 - PADOVA - ITALY, Italy

⁶ European Southern Observatory, Alonso de Cordova 3107 Vitacura Casilla 19001 Santiago, Chile

⁷ Istituto Nazionale di Astrofisica, Osservatorio Astronomico di Trieste, Via Tiepolo 11, I-34143 Trieste, Italy

⁸ European Southern Observatory, Karl-Schwarzschild-Str. 2 D-85748 Garching bei München

⁹ Università di Roma Tor Vergata, Via della Ricerca Scientifica, 1 00133 Rome, Italy

Received September 15, 1996; accepted March 16, 1997

ABSTRACT

Context. The Sagittarius dwarf Spheroidal Galaxy (Sgr dSph) provides us with a unique possibility of studying a dwarf galaxy merging event while still in progress. Moving along a short-period, quasi-polar orbit in the Milky Way Halo, Sgr dSph is being tidally dispersed along a huge stellar stream. Due to its low distance (25 kpc), the main body of Sgr dSph covers a vast area in the sky (roughly 15×7 degrees). Available photometric and spectroscopic studies have concentrated either on the central part of the galaxy or on the stellar stream, but the overwhelming majority of the galaxy body has never been probed.

Aims. The aim of the present study is twofold. On the one hand, to produce color magnitude diagrams across the extension of Sgr dSph to study its stellar populations, searching for age and/or composition gradients (or lack thereof). On the other hand, to derive spectroscopic low-resolution radial velocities for a subsample of stars to determine membership to Sgr dSph for the purpose of high resolution spectroscopic follow-up.

Methods. We used VIMOS@VLT to produce V and I photometry on 7 fields across the Sgr dSph minor and major axis, plus 3 more centered on the associated globular clusters Terzan 7, Terzan 8 and Arp 2. A last field has been centered on M 54, lying in the center of Sgr dSph. VIMOS high resolution spectroscopic mode has then been used to derive radial velocities for a subsample of the observed stars, concentrating on objects having colors and magnitudes compatible with the Sgr dSph red giant branch.

Results. We present photometry for 320,000 stars across the main body of Sgr dSph, one of the richest, and safely the most wide-angle sampling ever produced for this fundamental object. We also provide robust memberships for more than one hundred stars, whose high resolution spectroscopic analysis will be the object of forthcoming papers. Sgr dSph appears remarkably uniform among the observed fields. We confirm the presence of a main Sgr dSph population characterized roughly by the same metallicity of 47 Tuc, but we also found the presence of multiple populations on the peripheral fields of the galaxy, with a metallicity spanning from $[Fe/H]=-2.3$ to a nearly solar value.

Key words. Galaxies: Local Group – Galaxy individual: Sgr dSph – Galaxies: photometry – Galaxies: stellar content – Galaxy: globular clusters: individual: M 54

1. Introduction

Dwarf galaxy mergers are believed to play a key role in the buildup of the Milky Way (MW) Halo (Searle & Zinn, 1978; Carollo et al., 2007; Diemand et al., 2007). These are also invoked as suspect responsible of the appearance of the Thick Disk (Kroupa, 2002), of the Bulge/Bar system (Heller et al., 2007), and of the Disk warp (Ibata et al., 1997). The discovery of the Sagittarius dwarf Spheroidal galaxy (Sgr dSph; Ibata, Gilmore, & Irwin, 1994, 1995) allowed for the first time to observe the MW in the act of tidally accreting a dwarf galaxy. Immediately after the discovery, theoretical predictions

(Ibata et al., 1997; Helmi & White, 1999) as well as observational hints (Ibata et al., 1997; Ng, 1997; Ng & Schultheis, 1997; Ng, 1998; Majewski et al., 1999; Ivezić et al., 2000) concurred in indicating that Sgr dSph should be releasing its stellar content in the Halo along a massive, kinematically cold stream. The existence of the stream was finally confirmed by Ibata et al. (2001) and Majewski et al. (2003), and further branches of it were also identified in the stellar sample of the Sloan Digital Sky Survey (Newberg et al., 2003; Martínez-Delgado et al., 2004; Belokurov et al., 2006). As a matter of fact, the Sgr dSph stream is clearly the most prominent feature visible in the galactic Halo.

All such discoveries increased the importance of Sgr dSph not only as a “test case” of tidal merging, but as the source of a significant portion of the stellar population in the Halo. Majewski et al. (2003) estimated that roughly 75% of high-

Send offprint requests to: G. Giuffrida

[★] Based on observations made with ESO Telescopes at Paranal Observatory under programme ID 073.B-0455

latitude Halo M-giants originated from Sgr dSph debris, which also provided almost all Halo AGB C-stars (see Maunon et al., 2005). Zijlstra et al. (2006) estimated that up to 10% of the Halo material could come from Sgr dSph debris. A thorough reconstruction of the Sgr dSph stream(s), moreover, would pose very strong constraints on the shape of the MW dark matter Halo (e.g. Fellhauer et al., 2006). With the discovery of Sgr dSph, 4 globular clusters (GC) which were before considered belonging to the halo have been recognized as being associated with the Sgr dSph. While three of them (Terzan 7, Terzan 8, and Arp 2) lay at the outskirts of Sgr dSph, the position of the fourth one, M 54, coincides with the center of the dwarf spheroidal (Monaco et al., 2005B) although it likely formed elsewhere and fell subsequently into the galaxy core (Bellazzini et al., 2008). It became subsequently clear that a number of other globular clusters, currently lying far from Sgr dSph, have kinematical properties compatible with an origin within the Sgr dSph system, and a subsequent stripping (Bellazzini et al., 2003), or were actually embedded into the stream material (Martínez-Delgado et al., 2002). For at least one of them, Pal 12, the origin within the Sgr dSph system has now been firmly established (Cohen, 2004; Sbordone et al., 2007). The large Sgr dSph size (roughly 15×7 square degrees in the sky), a consequence of its modest distance (25 kpc, see Monaco et al., 2004), is likely the reason why only the central region of the galaxy, and the associated globular clusters, have been studied so far. M 54 and the surrounding area have been examined photometrically (e.g. Marconi et al., 1998; Bellazzini et al., 1999A,B; Layden & Sarajedini, 2000; Monaco et al., 2004; Bellazzini et al., 2006A; Siegel et al., 2007) as well as by means of high resolution spectroscopy (Bonifacio et al., 2000a, 2004; Tautvaišienė et al., 2004; Zaggia et al., 2004; Sbordone et al., 2005; Caffau et al., 2005; Monaco et al., 2005A; McWilliam & Smecker-Hane, 2005; Sbordone et al., 2007; Mottini et al., 2008). While ground based photometry suggests for the Sgr dSph main body population a mean metallicity of $[\text{Fe}/\text{H}] \sim -1$, spectroscopy shows a surprising abundance spread in the main body, with a significant population around $[\text{Fe}/\text{H}] = 0$, a mean value around $[\text{Fe}/\text{H}] = -0.5$ and a weak metal poor tail possibly extending below $[\text{Fe}/\text{H}] = -2.5$. The spectroscopic discovery of the metal rich population in the Sgr dSph core was then confirmed by the detection of its Turn Off superimposed over the M54 CMD in the HST ACS photometry by (Siegel et al., 2007). Globular clusters considered belonging to Sgr dSph spans a similar wide range in metallicity, from $[\text{Fe}/\text{H}] = -0.6$ for Terzan 7 to $[\text{Fe}/\text{H}] = -2.3$ for Terzan 8.

Stars in the Sgr dSph stream appear to be slightly less metal rich than those in the main body, with metallicity gradients along the stream (Bellazzini et al., 2006B; Clewley & Jarvis, 2006; Monaco et al., 2007; Chou et al., 2007). This would not be unexpected if the most metal poor stars were located in the outskirts of Sgr dSph and then subject to the tidal interaction with the MW.

The detailed chemical analysis of Sgr dSph population showed a highly peculiar abundance pattern, with anomalous abundances for a number of elements (Sbordone et al., 2007, and references therein). The detection of the same signature in Pal 12 was the concluding argument to assign the cluster to the Sgr dSph system.

Although it seems now established (e. g. Lanfranchi & Matteucci, 2007; Lanfranchi et al., 2006A,B) that galactic winds triggered by starbursts are required to explain the low $[\alpha/\text{Fe}]$ ratios observed in many dSph, the complete history of the Sgr dSph is far from being clarified. For instance, the extent to which Sgr dSph has been altered by the interaction

Table 1. List of observed fields

Field Name	Pos.	RA (J2000.0)	DEC (J2000.0)	l (deg)	b (deg)	VIMOS cameras
M 54	Cen	18:55:03.3	-30:28:41	5.954	-14.692	4
Sgr0	Min	18:56:12.9	-30:01:48	6.482	-14.743	4
Sgr1	Maj	18:43:00.0	-28:58:34	6.258	-11.689	4
Sgr2	Maj	18:48:56.1	-29:41:49	6.139	-13.165	3
Sgr3	Maj	19:00:57.6	-31:12:00	5.779	-16.140	3
Sgr4	Maj	19:07:00.0	-31:57:04	5.561	-17.615	3
Sgr5	Min	18:57:13.6	-29:35:24	6.990	-14.770	3
Sgr6	Min	18:52:44.6	-31:20:31	4.931	-14.581	4

with the MW is currently difficult to assess. The original mass of Sgr dSph is uncertain, as well as its original gas content. The large mass of the stream, the unusually high metallicity among the dSph, and the large population of GCs, are all indications that we are dealing with an object which was in the past more a dwarf elliptical than a “classic” dwarf spheroidal galaxy.

There is thus a number of open questions regarding this complex stellar system, some of which can only be addressed by the analysis of stellar populations *across* the main body of Sgr dSph. Among these open questions we will only mention the following: how did star formation proceed in Sgr dSph? How uniform is its chemical composition? Which is the lower limit of metallicity in Sgr dSph and does it show gradients in composition or age? What is the dynamics of the main body?

2. Observations

The program to sample the stellar populations across Sgr dSph was performed in three steps.

First, we secured VIMOS@VLT images of 7 fields across the major and minor axis of the galaxy, and of 5 fields for the associated GCs. Second, we selected targets to observe with the VIMOS Multi Object Spectroscopy (MOS) in the High Resolution red grism (645-860nm, R=2500) mode, with an exposure time of 600s for each pointing. Finally, we performed a follow-up spectroscopic analysis with FLAMES (GIRAFFE/UVES mode see Pasquini et al., 2000) on candidate Sgr dSph members in the 7 fields.

This paper presents the photometric study and the complete source catalog (available online) for the Sgr dSph main body fields. The results for Terzan 7, Terzan 8, Arp 2 and NGC 4147 will be presented in a forthcoming paper (Giuffrida et al., 2009), although the fiducial lines derived from that photometry will be employed here. The abundance and dynamical analysis from the high resolution spectra will be the object of a further paper.

Observations with VIMOS@VLT imaging camera (LeFevre et al., 2003) were obtained during 5 nights on March, April and May 2004. The instrument consists of four channels, each with a field of view of 7×8 arcmin and a pixel size of 0.205 arcsec, with a gap of about 2 arcmin between each quadrant.

Each pointing consists of two 10s exposures in the V and in the I band; the FWHM was in the range 0.7 to 1.3 arcsec. Tab. 1 presents the list of the observed fields. Last column indicates the number of channels used for each field because one of the VIMOS channels, Q1, turned out to be out of focus on the night 18-04-2004. Consequently for all fields observed that night, Sgr2, Sgr3, Sgr4 and Sgr5, only three channels, namely Q2, Q3 and Q4, could be used for photometry. The position of the fields is reported in Fig. 1, superimposed on a

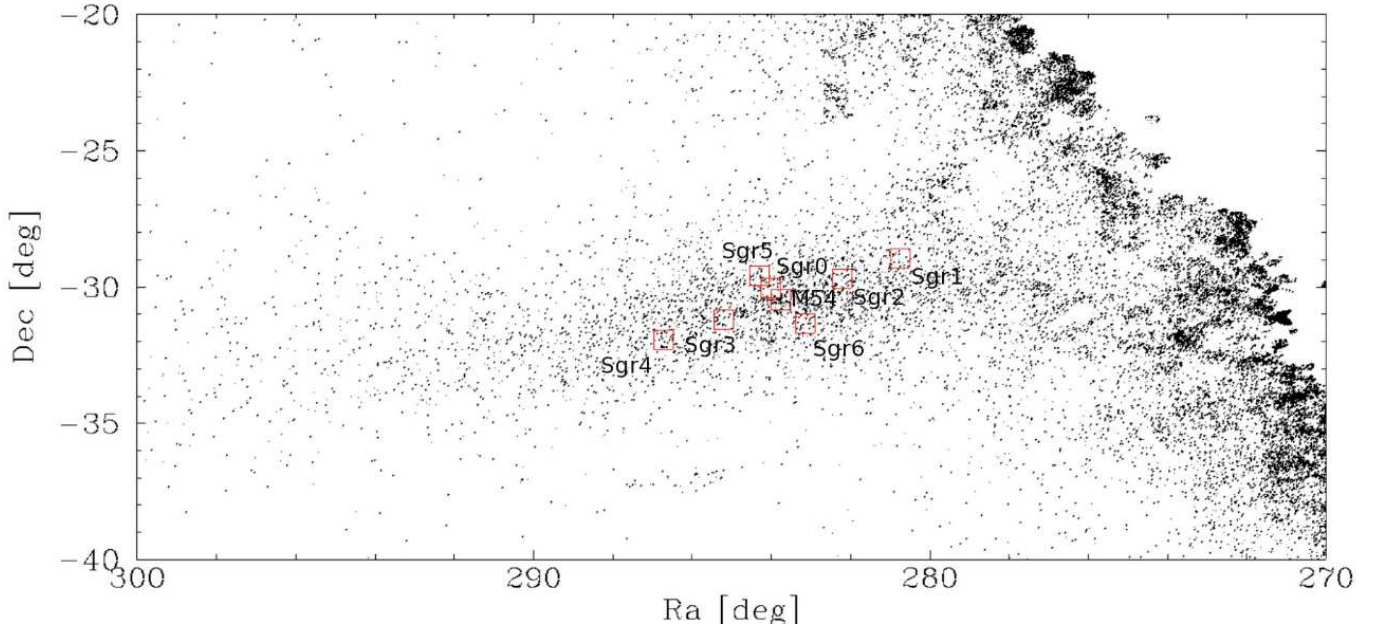


Fig. 1. Map of the Sgr dSph galaxy obtained from 2MASS and UCAC catalog selected in K, J–K, and E(B–V) ($E(B-V) < 0.555$, $0.95 < (J-K)_0 < 1.10$, $10.5 < K_0 < 12$, see Majewski et al. (2003)). The boxes shows the position of our fields

map of 2MASS and UCAC M-giants in the Sgr dSph region (see Majewski et al., 2003).

Concerning the pre-reduction, we applied to each frame overscan correction, bias subtraction and trimming according to the ESO-VIMOS pipeline. Fringing correction on I band frames was performed using IRAF tasks `imcombine` and `ccdproc`.

3. Data analysis

3.1. VIMOS Photometry

Photometry has been performed using the DAOPHOT/ALLFRAME packages (Stetson, 1994). Templates for the PSF have been selected in a semi-interactive mode, having selected a sample of bright stars uniformly distributed across the entire frame. The DAOPHOT task ‘`psf`’ has been used to model a first PSF which was used to perform a first photometry. The subsequent step has been to select from the catalogue so obtained a new sample of stars to model a more accurate PSF and to perform a second photometry on each individual frame. The photometric catalogs of the same field have been matched with DAOMATCH/DAOMASTER in order to perform the final photometry simultaneously in all the frames using ALLFRAME. DAOMASTER finally allowed us to obtain the catalogue for each field. The photometric calibration was performed using zero points obtained by the ESO Quality Control Team¹. Color terms have been derived through a set of standard stars observed during the same nights. The following correction was finally applied to the raw VIMOS photometry:

$$M = 2.5 * \log(\text{Flux}) - a * \text{Colour} + c_{ext} * \text{air} + Z_p + ap. \quad (1)$$

where a is the color term, air is the airmass, c_{ext} is the extinction coefficient, Z_p is the zero point and ap is the aperture correction.

¹ The measurements and values of the ZP for the observing nights of this program can be retrieved at the site <http://www.eso.org/observing/dfo/quality/>

3.2. Internal consistency

In order to check the internal consistency of our calibration, we selected, in each of our fields, a sample of bona-fide MW stars (stars in the interval $18.5 < V < 19.5$ and $0.8 < V-I < 1.05$) and corrected the catalogues according to the maps of interstellar reddening of Schlegel et al. (1998)², as corrected by Bonifacio et al. (2000b). A comparison of the color distribution of these stars (see Fig. 2) reveals a good homogeneity of our data.

3.3. VIMOS MOS spectroscopy

In order to obtain spectra with good and stable calibrations we implemented a new procedure to extract and calibrate VIMOS-MOS spectra and to derive reliable radial velocities, because the existing ESO-VIMOS pipeline (ver. 2.0.15, see Izzo et al. (2004)) produced output spectra which turned out to be unsatisfactory both in terms of extraction quality and wavelength calibration. Therefore we wrote an interactive procedure within the ESO pipeline which allows fine tuning of several parameters and better control of each calibration step. A typical VIMOS-MOS reduction consists of the following 5 steps:

1. `vmbias` to obtain a master bias frame;
2. `vmflat` to obtain the master screen flat and the not-normalised screen flat field;
3. `vmcaldisp` to produce an extraction table;
4. `vmstandard` to obtain the spectro-photometric table;
5. `vmobsstare` (or `vmobsbjitter` in case of jittered science exposures) to obtain the final reduced science exposure;

While steps 1–2, 4–5 do not present particular difficulties, the key passage is the 3rd step, i.e. the creation of a reliable extraction table. In our case the spectral distortions models, described in the input FITS headers, did not guarantee an accurate

² see <http://www.astro.princeton.edu/~Schlegel/dust/>

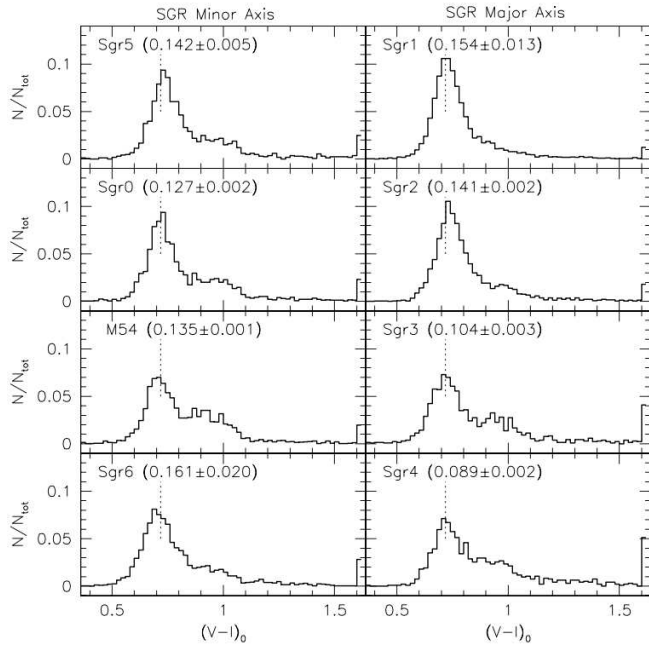


Fig. 2. Absolute $(V-I)_0$ color distribution of the MW sequence in the magnitude range $18.5 < V < 19.5$ for all the single fields. The magnitudes of each star has been de-reddened using values from Schlegel et al. (1998) corrected by Bonifacio et al. (2000b). The histograms are normalized to the total counts in the given magnitude range. The vertical dotted line shows the position of the maximum in the M 54 field, taken as a reference. In parenthesis the average value with rms scatter of $E(B-V)$ for the given field.

identification of the reference arc lamp lines and of the flat field spectra edges. Consequently we created a procedure to modify six recipe parameters until a good extraction table was obtained. According to our procedure the `MOS_SCIENCE_SKY` frame, containing the sky modeled for each slit spectrum, is used to perform the reduction quality check and derive for five selected skylines

$$diff = (Sky_{obs} - Sky_{exp}) \quad (2)$$

(where Sky_{obs} is the observed wavelength of the sky line and Sky_{exp} is the expected wavelength) for each line and for each slit. The accuracy in wavelength of the calibration is then estimated from the residuals. Typical values are of the order of 0.2 pixels.

Radial velocity of each star has been determined using the three lines of the Ca triplet (849.8, 854.2 and 866.2 nm) Typical uncertainty of the radial velocities obtained in this way varies from 10 to 20 km/s.

4. Comparison with previous photometry

As no overlap with data in literature exists for Sgr dSph peripheral fields, we used the photometry of the field around M 54 to check our calibration. In particular we used the photometry of Layden & Sarajedini (2000) (henceforth LS00) who worked on an area of 11.1×11.1 arcmin centered on M 54. In addition we used the standard stars of Stetson (2000) around NGC 4147 as his field partly overlaps with our observations in VIMOS quadrant 2.

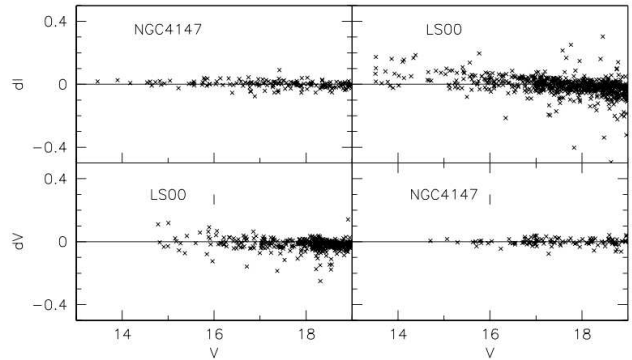


Fig. 3. Comparison between our photometry and references photometries. Difference in magnitude in V and I bands is plotted versus instrumental magnitudes. LS00 is Layden & Sarajedini (2000) and NGC 4147 are Stetson's standard stars.

Figures 3, 4 and 5 present the residuals between our photometry and the aforementioned studies for stars with $V < 19$ or $I < 19$. While a significant dispersion is clearly visible for LS00, the comparison with NGC 4147 shows a good photometric agreement and the absence of obvious trends with the position of the stars (the root mean square for V data is about 0.025 with a sample of 109 stars, for I data is about 0.023 with a sample of 159 stars).

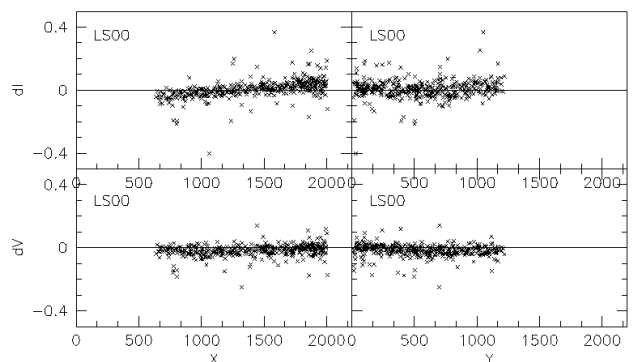


Fig. 4. Comparison between our photometry and reference photometry LS00. Difference in magnitude in V and I bands is plotted versus X and Y coordinates in pixel of the stars. Only stars with $V < 19$ or $I < 19$ have been plotted LS00 is Layden & Sarajedini (2000)

Actually two additional photometric studies exist, namely those of Marconi et al. (1998) and Monaco et al. (2002). However considering that the first one covers a small area of the sky (5.6×5.7 arcmin) and that the second one is based on WIF@ESO2.2 data which is known to suffer of significant inho-

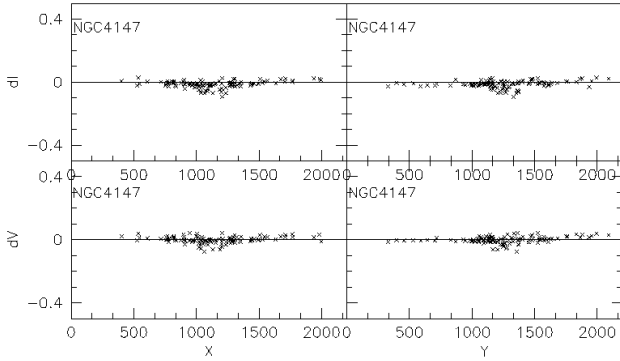


Fig. 5. Comparison between our photometry and reference photometry on NGC 4147. Difference in magnitude in V and I bands is plotted versus X and Y coordinates in pixel of the stars. Only stars with $V < 19$ or $I < 19$ have been plotted.

mogeneity (Koch et al., 2004; Calamida et al., 2008) we didn't consider useful to perform such comparisons. In conclusion, of the two studies we compared with, one (Stetson) supports our calibration while the other (LS00) presents trends both in position and in magnitude which are impossible to disentangle at the moment. All in all the comparisons did not offer particular reasons to question our calibration.

5. Color Magnitude Diagrams

In Fig. 6 we present the CMDs of the seven Sgr dSph peripheral fields plus the field centered on M 54. Fields along the minor and major axis are presented in the left and in the right panel respectively. Inspection of the CMDs reveals immediately that:

- contamination of the disk of the Milky Way is visible as a roughly vertical sequence at $V-I \approx 0.8$ and from $V=20.5$ to $V=13.5$. The giant branch of the old Bulge population is visible as a second sequence, nearly parallel to the previous one, at $V-I \approx 1.0$.
- A very similar galactic contamination can be observed in all the minor axis fields, which are centered at nearly constant galactic latitude. The fields along the major axis show a galactic contamination which dramatically increases from field Sgr 4 to field Sgr 1;
- the turn off of the Sgr main population is clearly detectable in all fields at a magnitude between $V=20.5$ and $V=21.5$ and color $V-I \approx 0.8$.
- a densely populated red clump at $V \approx 18.0$ and $V-I \approx 1.2$ is detectable in all fields;
- the Red Giant Branch (RGB) of Sgr dSph main population is clearly present in field Sgr 2, 3, 5, 6 and in the M 54 field. In Sgr 1 and Sgr 4 the number of RGB stars is lower, but the RGB remains nevertheless detectable;
- an extended Blue Plume (BP) is visible in all fields in the intervals $0.4 < V-I < 0.8$ and $19.0 < V < 21.0$. This population, which is clearly visible in the fields M 54, Sgr 0, 5, and 6, is considered to be the Main Sequence of the younger, metal rich population of Sgr dSph (Bonifacio et al., 2000a, 2004; Siegel et al., 2007; Sbordone et al., 2007). The alternative interpretation of the plume as a sequence of Blue Stragglers cannot be ruled out (see discussion in Momany et al., 2007).

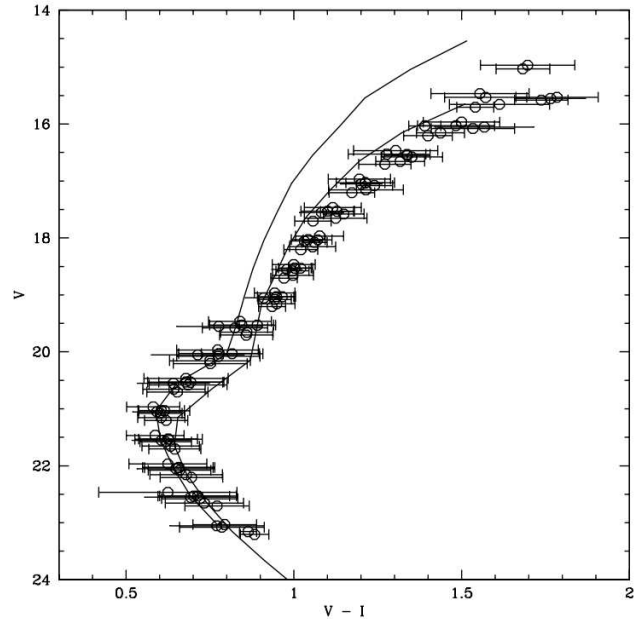


Fig. 7. Sgr dSph main population position on Sgr dSph fields with uncertainties in color. Fiducial lines of 2 galactic globular cluster are superimposed: M5 and 47Tuc characterized by $[Fe/H] = -1.24, -0.67$

6. Sgr dSph main population

All the Sgr dSph fields are characterized by the presence of a dominant population whose progeny is the ubiquitous RGB. To investigate the possible presence of population gradients along the major and minor axes we carried out a comparison of the position of the RGB in each field.

After having derived fiducial line of the main population in each field and having corrected for reddening differences, we plotted all the fiducial lines in Fig. 7 as open circles (Sgr1 was not reported because the high contamination of the MW did not allow to draw a reliable fiducial line). RGB positions, used for the fiducial lines, and associated uncertainties are calculated finding the median value of the color distribution of stars on each magnitude interval around the expected position of the RGB, SGB and main sequence, and fitting with a gaussian the distribution around the median value. On the same figure the fiducial lines of M5 and 47Tuc are drawn. A simple inspection of Fig. 7 reveals that:

1. Within the uncertainties the dominant population of Sgr dSph is similar across the field.
2. Metallicity of Sgr dSph main population is comparable with that of 47Tuc ($[Fe/H] = -0.67$), confirming previous estimates;

7. Looking for other populations

From VIMOS-MOS observations we acquired spectra for 1000 stars, and we selected 180 candidate Sgr dSph members from radial velocities centered on the 7 Sgr dSph fields. 575 targets have been added to this sample selecting other stars near in color and magnitude to the 180 confirmed Sgr dSph members. Finally FLAMES followup has been performed on these stars. After having measured radial velocities for these stars we

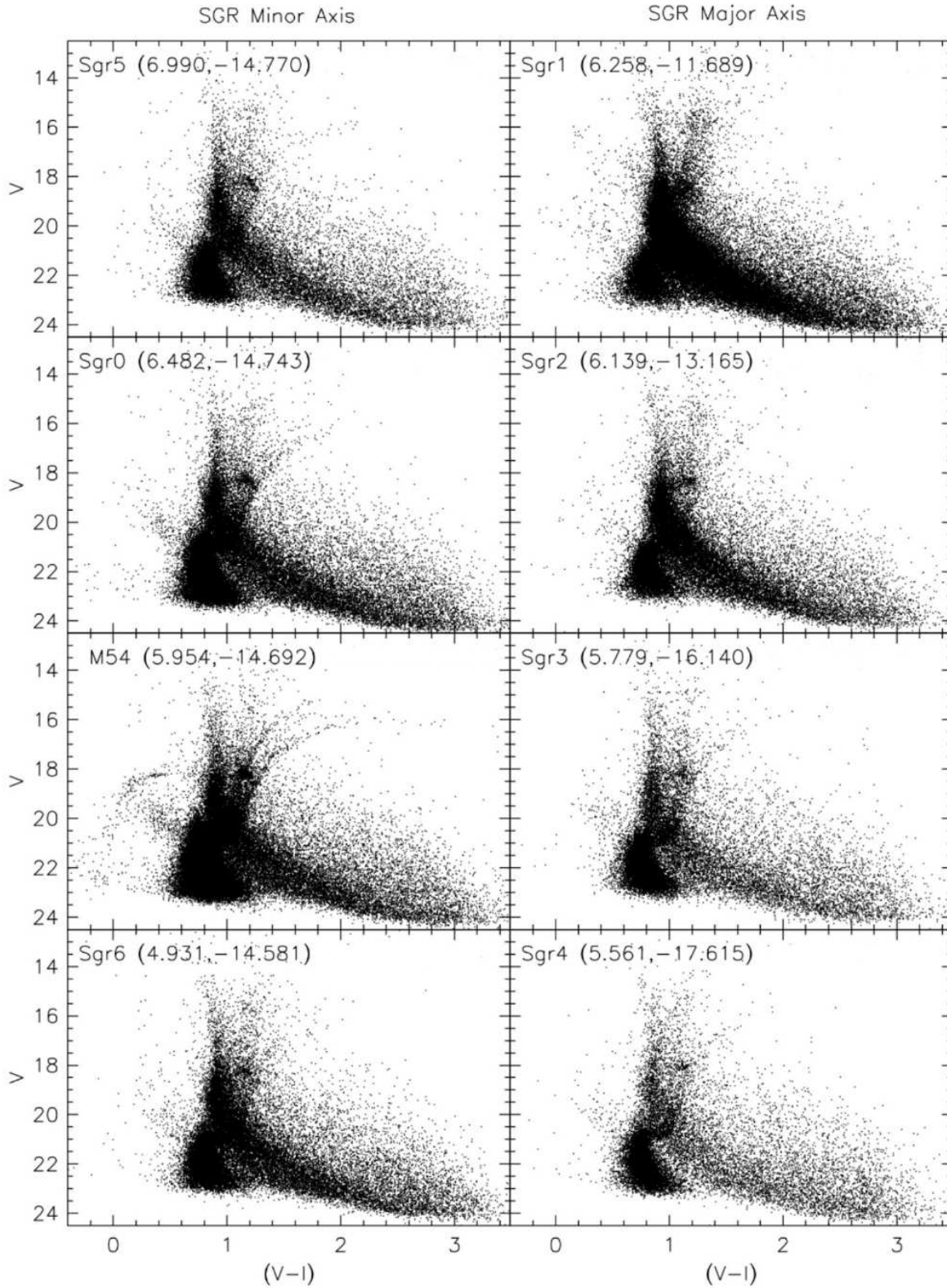


Fig. 6. VIMOS Colour-Magnitude Diagrams (CMDs) for all observed field. Each box shows the name of the field and the galactic coordinates in parenthesis. **Left column:** CMD of the fields on the center (M54) and along the Minor Axis of SGR. **Right column:** CMDs of the fields along the Major Axis of SGR.

Table 2. V - (V-I) fiducial lines for the globular clusters M 92, M 5, 47 Tuc, .

V mag	V-I M 92	V-I M 5	V-I 47 Tuc	V-I
12.0		1.557	1.566	
12.5		1.389	1.378	
13.0	1.180	1.253	1.251	
13.5	1.077	1.178	1.165	
14.0	1.023	1.098	1.090	
14.5	0.963	1.034	1.039	
15.0	0.928	0.992	1.000	
15.5	0.894	0.952	0.959	
16.0	0.859	0.919	0.942	
16.5	0.841	0.893	0.925	
17.0	0.815	0.869	0.812	
17.5	0.783	0.840	0.709	
18.0	0.638	0.694	0.699	
18.5	0.564	0.630	0.735	
19.0	0.571	0.644	0.795	
19.5	0.605	0.683	0.867	
20.0	0.653	0.734	0.964	
20.5	0.714	0.814	1.067	
21.0	0.788			
21.5	0.899			
22.0	0.957			
22.5				

Table 3. V - (V-I) fiducial lines for the globular clusters M 54, Terzan 7, Terzan 8, Arp 2.

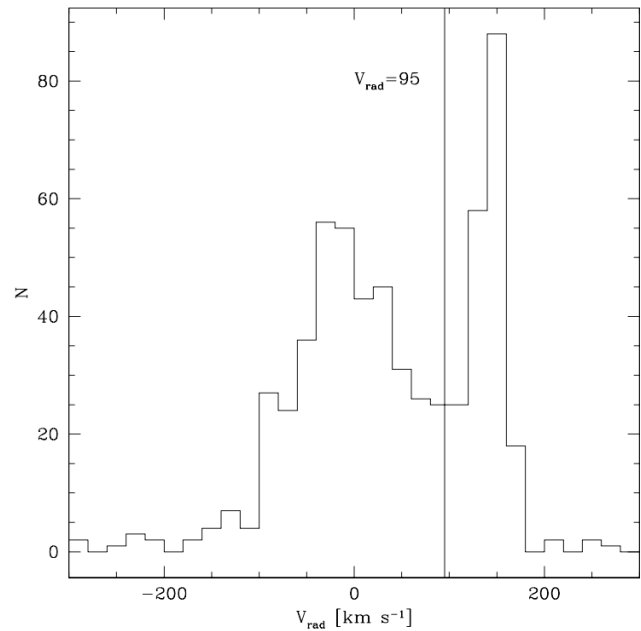
V mag	V-I M 54	V-I Ter 7	V-I Ter 8	V-I Arp 2
15.5	1.631	—	—	—
16.0	1.440	1.425	1.349	1.299
16.5	1.340	1.294	1.222	1.215
17.0	1.254	1.219	1.150	1.109
17.5	1.197	1.148	1.104	1.072
18.0	1.145	1.067	1.064	1.019
18.5	1.104	1.047	1.032	0.981
19.0	1.067	0.992	0.999	0.948
19.5	1.049	0.958	0.978	0.927
20.0	1.010	0.933	0.948	0.896
20.5	1.020	0.731	0.926	0.866
21.0	0.806	0.660	0.755	0.781
21.5	0.776	0.670	0.683	0.659
22.0	0.794	0.701	0.670	0.672
22.5	0.832	0.758	0.732	0.715
23.0	0.879	0.816	0.774	0.778
23.5	0.911	0.897	0.820	0.820

plotted these velocities in the histogram of Fig. 8. We have then selected the sample with $V_{rad} > 95$ because we considered that the large majority of this sample is constituted by Sgr dSph stars. The full analysis of the FLAMES sample will be presented in Sbordone et al., 2009. The stars selected in this way are reported as black dots in Fig. 9, in addition to the complete photometry of the present paper and with the superimposed fiducial lines of M 92, M 5 and 47 Tuc (based on the photometry of (Stetson, 2000)). Inspection of Fig. 9 reveals that the sample selected on the basis of radial velocity span a large interval of metallicity, with stars more metal rich than 47 Tuc ($[Fe/H]=-0.67$), and stars more metal poor than M92 ($[Fe/H]=-2.52$). These results are in agreement with the data collected on the Sgr dSph core (Zaggia et al., 2004; Monaco et al., 2005A; McWilliam & Smecker-Hane, 2005; Sbordone et al., 2007), with two remarkable exceptions, namely the presence of a well populated intermediate population ($[Fe/H]$ around -1) and a large numbers of bright stars lying at the blue edge of the RGB ($17 < V < 14$ and $0.9 < V-I < 1.1$) that cannot be reproduced with a “M 92 like” population. The case of these stars will be analyzed in the next section.

The comparison of the fiducial lines for Sgr dSph globular clusters M 54, Terzan 7, Terzan 8, and Arp 2 in Fig. 10 reveals a similar scenario: Terzan 7 is not sufficiently metal rich to trace the most metal rich Sgr dSph population and the Terzan 8 fiducial line is not compatible with the position of the bright stars at the blue edge of the RGB.

7.1. RGB Blue edge

In order to investigate on the nature of the stars in the region ($17 < V < 14$ and $0.9 < V-I < 1.1$) we overplotted a 14 GYr $[Fe/H]=-3.3$ isochrone to the CMD (S. Cassisi, private communication). Inspection of Fig. 11, however, rules out the hypothesis that the observed stars at the blue edge of the RGB are representative of an extremely metal poor population, essentially for

**Fig. 8.** Radial velocity distribution of the FLAMES sample. All stars with $V_{rad} > 95$ km/s are candidate Sgr dSph members**Table 4.** Reddening, Distance modulus and metallicity of the 3 Galactic globular clusters. (Harris, 1996; King et al., 1998; Carretta et al., 2004; Yong et al., 2008)

Object	$E(B-V)$	$(m-M)_V$	$[Fe/H]$
M92	0.02	14.64	-2.52
M5	0.03	14.46	-1.24
47Tuc	0.04	13.37	-0.67

the anomalous expected position of the main sequence and turn off.

On the other hand, in this region of the cmd a significant contamination of the stars in the MW Bulge is expected, and the question is whether the radial velocities we have measured may exclude they belong to the MW. In order to clarify this point we

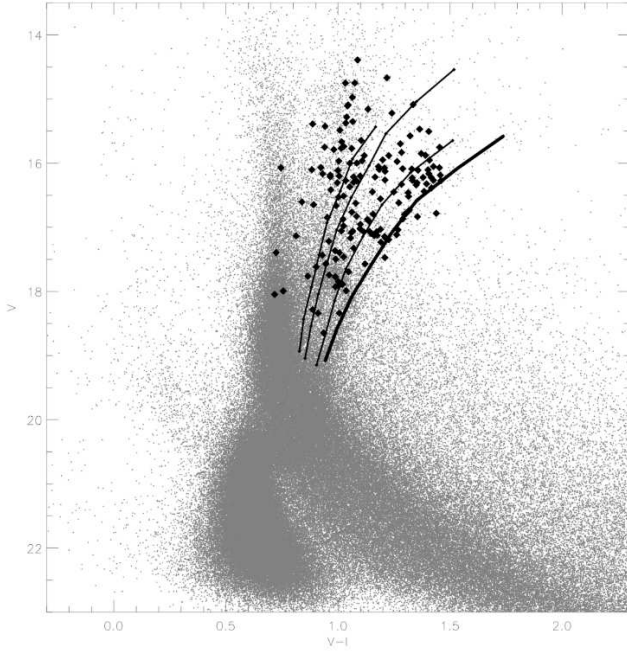


Fig. 9. Colour-magnitude diagram for all the stars detected on the 7 Sgr dSph peripheral fields with overplotted the stars observed with FLAMES and showing radial velocities compatible with a membership in Sgr dSph. Fiducial lines of 3 galactic globular cluster are superimposed. From left to right : M92, M5 and 47Tuc characterized by $[Fe/H] = -2.52, -1.24, -0.67$. The bold line follows the position of the RGB of Sgr dSph main population.

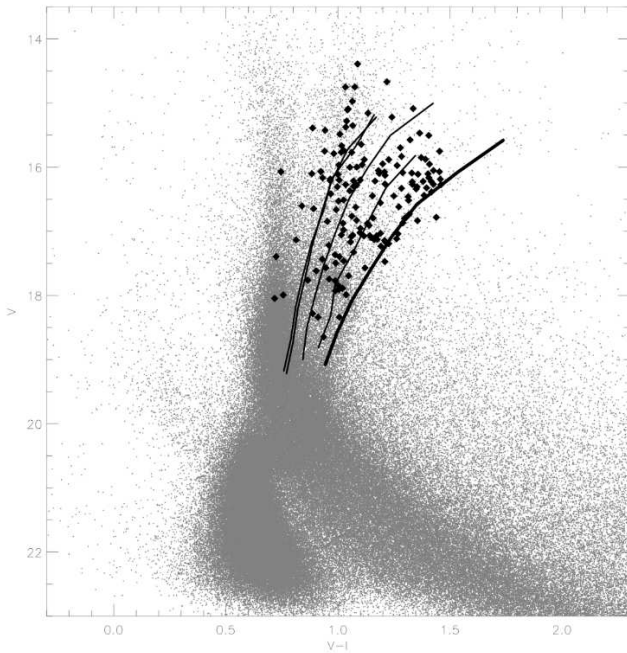


Fig. 10. Colour-magnitude diagram for all the stars detected on the 7 Sgr dSph peripheral fields with overplotted the stars observed with FLAMES and showing radial velocities compatible with a membership in Sgr dSph. Fiducial lines of 4 Sgr dSph globular clusters are superimposed. From left to right : Ter8, Arp2, M54, Ter7 characterized by $[Fe/H] = -2.34, -1.83, -1.55, -0.6$. The bold line follows the position of the RGB of Sgr dSph main population.

Table 5. Reddening, Distance modulus and metallicity of the 4 Sgr dSph globular clusters. (Harris, 1996; Brown et al., 1999; Monaco et al., 2004; Sbordone et al., 2007; Mottini et al., 2008)

Object	$E(B-V)$	$(m-M)_V$	$[Fe/H]$
Ter8	0.12	17.45	-2.34
Arp2	0.10	17.59	-1.83
M54	0.15	17.10	-1.55
Ter7	0.07	17.05	-0.60

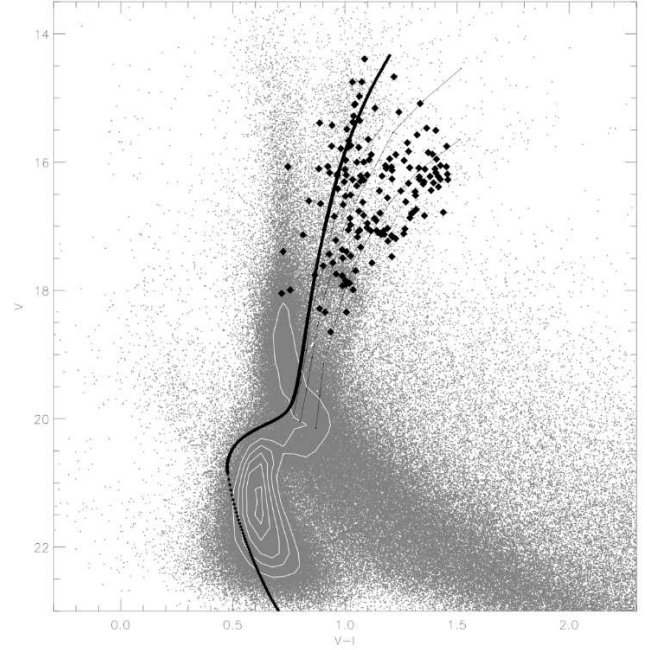


Fig. 11. Colour-magnitude diagram for all the stars detected on the 7 Sgr dSph peripheral fields with overplotted the stars observed with FLAMES and showing radial velocities compatible with a membership in Sgr dSph. Fiducial lines of the galactic globular clusters and isochrone characterized by 14 Gyr $[Fe/H] = -3.3$ are superimposed. Iso-density contours are superimposed on the Sgr dSph main sequence region.

have plotted in Fig. 12 the distribution of radial velocities of the Besançon sample (Robin et al., 2004) for MW stars. Inspection of Fig. 12 reveals immediately that the tail of the distribution, namely about the 20 % of the sample, fall in the region of the radial velocity of Sgr dSph. We can then conclude that the “RGB Blue edge stars” are indeed heavily contaminated by Bulge stars and there is the possibility that all of them are Bulge stars. It cannot be excluded however that a fraction of them belongs to an extremely metal poor Sgr dSph population.

8. Discussion and Conclusions

In this paper we present a V, I VIMOS photometric catalog for ~ 320000 sources across eight fields in the direction of the Sagittarius dwarf Spheroidal galaxy, covering roughly 0.43 square degrees. The main purpose of this survey was to probe Sgr dSph stellar populations over a significant fraction of its spatial extension, from its center to its periphery, and to provide targets for high resolution spectroscopical analysis.

Our survey extends over 6.2 degrees along the galaxy major axis, and 2 degrees along the minor axis, i.e. about one third

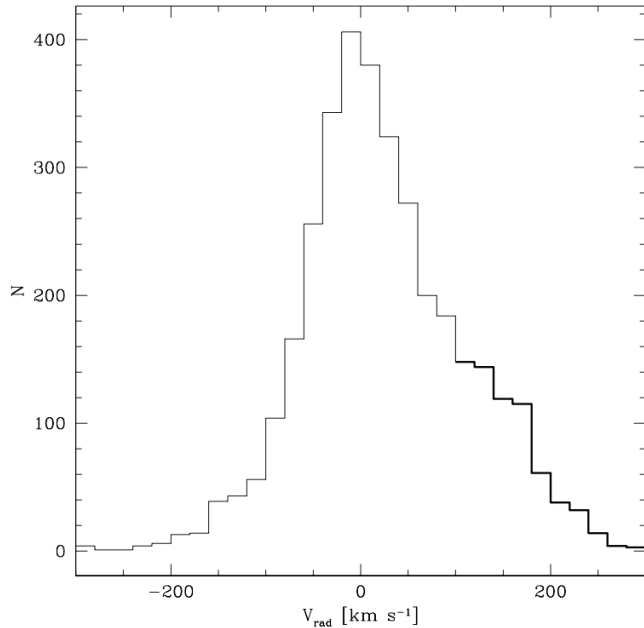


Fig. 12. Radial velocity distribution of the Besançon simulated sample in the “RGB Blue edge” box. The Sgr dSph velocity compatible stars are plotted in bold.

of Sgr dSph extension. Two occurrences limit the extension of this sort of studies: first the presence of the MW disk which makes the contamination too severe at the position of our field Sgr 1, second the fact that the density of Sgr dSph stars drops quickly when moving away from the center, making a spectroscopic follow-up highly inefficient. During the FLAMES follow-up observations, in fields such as Sgr 1, Sgr4, Sgr 5, and Sgr 6 we were able to place only a few dozens of fibers on “radial velocity members” detected by VIMOS-MOS. VIMOS spectroscopy provided radial velocities adequate for FLAMES candidates selection, but not good enough for dynamical analysis. The uncertainties in the MOS wavelength calibration, together with the limited S/N of the spectra led to a final uncertainty of about 10–20 km s⁻¹, comparable to the overall Sgr dSph velocity dispersion (see Fig. 8).

Within the precision allowed by the mentioned MW contamination, the population of Sgr dSph appears remarkably uniform among the observed fields. We thus confirm the presence of a main Sgr dSph population characterized roughly by the same metallicity of 47 Tuc, but we also found the presence of multiple populations on the peripheral fields Sgr0-Sgr6, with a metallicity spanning from [Fe/H]=−2.3 to a nearly solar value. Our research thus confirms the extremely complex evolution of this object. Using our FLAMES data we plan to better characterize these populations both from a chemical and a dynamical point of view, adding new pieces to this intriguing puzzle.

Acknowledgements. The authors L.S. and P.B. acknowledge financial support from EU contract MEXT-CT-2004-014265 (CIFIST). We thank S. Cassisi for providing us an unpublished low metallicity isochrone. This research has made use of the VizieR Service (Ochsenbein et al., 2000) operated at CDS, Strasbourg, France, and of NASA’s Astrophysics Data System.

References

Bellazzini, M., et al. 2008, ArXiv e-prints, 807, arXiv:0807.0105

- Bellazzini, M., Correnti, M., Ferraro, F. R., Monaco, L., & Montegriffo, P. 2006 A, A&A, 446, L1
- Bellazzini, M., Newberg, H. J., Correnti, M., Ferraro, F. R., & Monaco, L. 2006 B, A&A, 457, L21
- Bellazzini, M., Ferraro, F. R., & Ibata, R. 2003, AJ, 125, 188
- Bellazzini, M., Ferraro, F. R., & Buonanno, R. 1999 A, MNRAS, 304, 633
- Bellazzini, M., Ferraro, F. R., & Buonanno, R. 1999 B, MNRAS, 307, 619
- Belokurov, V., et al. 2006, ApJ, 642, L137
- Bonifacio, P., Sbordone, L., Marconi, G., Pasquini, L., & Hill, V. 2004, A&A, 414, 503
- Bonifacio, P., Hill, V., Molaro, P., Pasquini, L., Di Marcantonio, P., & Santini, P. 2000, A&A, 359, 663
- Bonifacio, P., Monai, S., & Beers, T. C. 2000, AJ, 120, 2065
- Brown, J. A., Wallerstein, G., & Gonzalez, G. 1999, AJ, 118, 1245
- Caffau, E., Bonifacio, P., Faraggiana, R., & Sbordone, L. 2005, A&A, 436, L9
- Calamida, A., Corsi, C. E., Bono, G., Stetson, P. B., Freyhammer, L. M., & Buonanno, R. 2008, arXiv:0801.0693
- Carollo, D., et al. 2007, Nature, 450, 1020
- Carretta, E., Gratton, R. G., Bragaglia, A., Bonifacio, P., & Pasquini, L. 2004, A&A, 416, 925
- Chou, M.-Y., et al. 2007, ApJ, 670, 34
- Clewley, L., & Jarvis, M. J. 2006, MNRAS, 368, 310
- Cohen, J. G. 2004, AJ, 127, 1545
- Diemand, J., Kuhlen, M., & Madau, P. 2007, ApJ, 667, 859
- Fellhauer, M., et al. 2006, ApJ, 651, 167
- Giuffrida, G., et al., 2009, in preparation
- Gray N., et al., 2005, Astronomical Data Analysis Software and Systems XIV, 347, 119
- Harris, W. E. 1996, AJ, 112, 1487
- Heller, C. H., Shlosman, I., & Athanassoula, E. 2007, ApJ, 671, 226
- Helmi, A., & White, S. D. M. 1999, MNRAS, 307, 495
- Ibata, R., Lewis, G. F., Irwin, M., Totten, E., & Quinn, T. 2001, ApJ, 551, 294
- Ibata, R. A., Wyse, R. F. G., Gilmore, G., Irwin, M. J., & Suntzeff, N. B. 1997, AJ, 113, 634
- Ibata, R. A., Gilmore, G., & Irwin, M. J. 1995, MNRAS, 277, 781
- Ibata, R. A., Gilmore, G., & Irwin, M. J. 1994, Nature, 370, 194
- Ivezić, Ž., et al. 2000, AJ, 120, 963
- Izzo, C., Kornweibel, N., McKay, D., Palsa, R., Peron, M., & Taylor, M. 2004, The Messenger, 117, 33
- King, J. R., Stephens, A., Boesgaard, A. M., & Deliyannis, C. 1998, AJ, 115, 666
- Koch, A., Odenkirchen, M., Grebel, E. K., & Caldwell, J. A. R. 2004, Astronomische Nachrichten, 325, 299
- Kroupa, P. 2002, MNRAS, 330, 707
- Landolt, A. U. 1992, AJ, 104, 340
- Lanfranchi, G. A., Matteucci, F., & Cescutti, G. 2008, A&A, 481, 635
- Lanfranchi, G. A., & Matteucci, F. 2007, A&A, 468, 927
- Lanfranchi, G. A., Matteucci, F., & Cescutti, G. 2006 A, A&A, 453, 67
- Lanfranchi, G. A., Matteucci, F., & Cescutti, G. 2006 B, MNRAS, 365, 477
- Law, D. R., Majewski, S. R., & Johnston, K. V. 2009, ApJL in press, arXiv:0908.3187
- Layden, A. C., & Sarajedini, A. 2000, AJ, 119, 1760
- LeFevre, O., et al. 2003, Proc. SPIE, 4841, 1670
- Majewski, S. R., Skrutskie, M. F., Weinberg, M. D., & Ostheimer, J. C. 2003, ApJ, 599, 1082
- Majewski, S. R., et al., 1999, AJ, 118, 1709
- Marconi, G., Buonanno, R., Castellani, M., Iannicola, G., Molaro, P., Pasquini, L., & Pulone, L. 1998, A&A, 330, 453
- Martínez-Delgado, D., Gómez-Flechoso, M. Á., Aparicio, A., & Carrera, R. 2004, ApJ, 601, 242
- Martínez-Delgado, D., Zinn, R., Carrera, R., & Gallart, C. 2002, ApJ, 573, L19
- Mauron, N., Kendall, T. R., & Gigoyan, K. 2005, A&A, 438, 867
- McWilliam, A., & Smecker-Hane, T. A. 2005, ApJ, 622, L29
- Momany, Y., Held, E. V., Saviane, I., Zaggia, S., Rizzi, L., & Gullieuszik, M. 2007, A&A, 468, 973
- Monaco, L., Bellazzini, M., Bonifacio, P., Buzzoni, A., Ferraro, F. R., Marconi, G., Sbordone, L., & Zaggia, S. 2007, A&A, 464, 201
- Monaco, L., Bellazzini, M., Bonifacio, P., Ferraro, F. R., Marconi, G., Pancino, E., Sbordone, L., & Zaggia, S. 2005 A, A&A, 441, 141
- Monaco, L., Bellazzini, M., Ferraro, F. R., & Pancino, E. 2005 B, MNRAS, 356, 1396
- Monaco, L., Bellazzini, M., Ferraro, F. R., & Pancino, E. 2004, MNRAS, 353, 874
- Monaco, L., Ferraro, F. R., Bellazzini, M., & Pancino, E. 2002, ApJ, 578, L47
- Monai, S., Bonifacio, P., & Sbordone, L. 2005, A&A, 433, 241
- Mottini, M., Wallerstein, G., & McWilliam, A. 2008, AJ, 136, 614
- Newberg, H. J., et al. 2003, ApJ, 596, L191
- Ng, Y. K. 1998, A&A, 338, 435

'Arp 2' on page 7
'Terzan 7' on page 7
'Sgr dSph' on page 7
'Terzan 8' on page 7
'M 54' on page 7
'Terzan 7' on page 7
'Terzan 8' on page 7
'Arp 2' on page 7
'M 54' on page 7
'Ter 7' on page 7
'Ter 8' on page 7
'Arp 2' on page 7
'Sgr dSph' on page 7
'Sgr dSph' on page 8
'Sgr dSph' on page 8
'M92' on page 8
'M5' on page 8
'47Tuc' on page 8
'Sgr dSph' on page 8
'Ter8' on page 8
'Arp2' on page 8
'M54' on page 8
'Ter7' on page 8
'Sgr dSph' on page 9
'Sgr dSph' on page 9